

A Resilient Extractor for Electro spray Arrays

IEPC-2022-206

*Presented at the 37th International Electric Propulsion Conference
Massachusetts Institute of Technology, Cambridge, MA, USA
June 19-23, 2022*

Collin B. Whittaker¹, Henry A. Sodano², and Benjamin A. Jorns³
University of Michigan, Ann Arbor, Michigan, 48109

A concept for a resilient electro spray extractor architecture that is robust to arcing is motivated and demonstrated experimentally. In this concept, a thin metallized film is deposited on a thick dielectric frame, which is placed directly on top of a standard emitter surface. This rigid structure ensures a high degree (10 μm) uniformity of extractor to surface emitter distance over the entire thruster area. Similarly, if arcs occur due to propellant deposition, the thin film that conducts the localized current is ablated, removing itself from the circuit. A 576-aperture prototype is manufactured using a CNC mill and DC magnetron sputterer and the extractor installed within an electro spray thruster based on the Air Force Research Laboratory's AFET-2 design. The thruster with the resilient extractor is shown to operate stably in a vacuum facility up to 2700 V in negative DC mode while the current is approximately 10% of the baseline AFET-2 design. This disparity is attributed largely to differences in the fabrication of the emitters rather than the resilient extractor. Micrographs of the extractor surface before and after operation are taken with an optical microscope. It is found that propellant was deposited on the face of approximately 8% of the extractor apertures. Shorts from this deposition resulted in the local removal of the metal film and the thruster was able to continue operation with little interruption, in accordance with its concept of operation. The performance of the prototype is examined within the context of potential large-scale (>100 W) electro spray systems.

I. Introduction

ELECTROSPRAY is a process wherein a conducting fluid meniscus subject to strong electric fields deforms into a sharp cone-like structure that sheds charge from its apex. Of its manifold applications, perhaps the most exciting is its use as a form of electric propulsion, where its ionic liquid propellants offer several potential advantages over plasma-based technologies like Hall thrusters and ion thrusters, most crucially avoiding wall losses associated with operating at high surface area to volume ratios (i.e. at smaller scales). Indeed, because the physics underlying electro spray are nano- to micro-scale phenomena, individual emitters can be manufactured at the microscale, providing key capability for micropropulsive applications [1]. Though individual electro sprays exhibit greater thrust per unit area than virtually any other EP technology as a result, the thrust they produce is still small [2], and it is necessary to leverage microelectromechanical scale (MEMS) or similar processes to manufacture many individual electro spray emitters in parallel to meet mission needs [3–5], in principle scaling to arbitrary size.

To date, however, systems have yet to be demonstrated in excess of $\sim O(1)\text{W}$ of power (cf. [1, 3, 6, 7]). While there are several confounding factors in electro spray development, including uncertain physics like the onset of multiple emission cites [8, 9], two of the most important factors are a result of a common architecture in electro spray systems. Firstly, electro spray emitters are typically needle-like structures aligned to a corresponding perforation in an electrode suspended over them, which may simply be a thin sheet of metal [3, 10, 11] or a coated wafer [5, 6]. While such systems are simple to align at small scale, when considering a larger system, flexure in the electrode and similar inhomogeneities can potentially remove this alignment and cause variability in performance between emitters [10, 12]. Secondly, and relatedly, this can acutely exacerbate the arcing or backspray failure modes of electro spray, wherein propellant deposition

¹PhD Candidate, Aerospace Engineering, cbwhitt@umich.edu

²Professor, Aerospace Engineering

³Associate Professor, Aerospace Engineering

on the extractor electrode shorts it to the emitters, preventing continued operation [1, 13]. The practical consequence of this variability is that a small proportion of errant emitters can precipitously decrease expected device lifetimes as arrays are made larger [11, 13, 14].

One key to addressing this difficulty is seeking emitter designs robust to these tolerances, such that they behave acceptably even at off-nominal designs [15]. However, in parallel to this preventative solution we seek also a mitigative one. that is, to identify an architecture designed to be less subject to these inhomogeneities and for which the failure of a single emitter does not disable the entire array. One way to do so is to provide a means by which individual emitters can be removed from the circuit as they fail, allowing the remainder to continue to operate. The simplest such method would be to electrically isolate the emitters, so that each is supplied power individually. While this would ensure that a localized short only disables a single emitter, this would also mean that an array would require as many power supplies as it had emitters, a prohibitive penalty.

An alternative methodology leverages the materials science of supercapacitors, which often consist of many sandwiched layers of metallized dielectric. If a short develops between two layers, the inrush current is sufficient to locally ablate the metallization, leaving a non-conducting hole between the sheets and allowing the capacitor to continue operation. Given the need for solutions to this problem and the success this method has had in other fields, there is a strong incentive to explore its applicability to electrospray devices.

Correspondingly, in this work we present the characterization of an electrospray extractor utilizing this technology. This paper is organized in the following way. In Sec. II, we describe the concept underlying the resilient electrode and detail the manufacture of a test article. We follow this in Sec. III with a description of the experimental facility and methodologies used to characterize it. We then present in Sec. IV a current-voltage map of the thruster operating with the resilient extractor and contrast the performance presented here with that of the same thruster using a more traditional electrode. We also there describe its response to shorts between the extractor and emitter electrodes. Lastly, in Sec. V, we discuss our results within the context of the viability of this technology.

II. Extractor Fabrication and Integration

In this section, we first describe the concept of the resilient extractor. Then, we describe the fabrication of an extractor prototype test article. Finally, we describe the integration of this prototype into a thruster in preparation for experimentation.

A. Resilient extractor concept

Figure 1 shows the principle of the resilient extractor design. A thin conducting film (e.g. silver) is deposited on a comparatively thick dielectric frame, providing an equipotential surface to generate the extraction field for an electrospray. This frame interfaces directly atop an emitter chip (shown here as porous-type) and insodoing automatically enforces the gap distance between the electrodes and aids in laterally aligning the apertures. Additionally, the thick form of the extractor chip and its mate to the emitter chip stiffens the construction to prevent bowing in the electrode. In the event that propellant causes a local short between the extractor electrode and the emitter, the large inrush of current resulting from the finite capacitance of the electrodes deposits energy in the surrounding grid, causing an ablation of the conducting film and removing the current path. Thus, the architecture would aid alignment, promote emission uniformity, and provide innate and passive fault tolerance to the system.

B. Fabrication of test articles

We constructed a test extractor of this architecture designed to be compatible with the Air Force Research Laboratory's AFET-2 thruster. While the design and manufacturing methodologies underlying the AFET-2 are discussed in greater detail elsewhere [3], we review them briefly here, as we constructed our own copy of the thruster for use in these tests. The central component of the AFET-2 is a chip of 576 square pyramidal electrospray emitters made of porous borosilicate glass. This emitter chip is stacked onto a porous glass reservoir with a filter paper as an interface and compressed by a spring against a distal electrode which sits at the surface of the emitter chip. This stack is housed within a dielectric frame, forming a propellant module. This propellant module sits inside a larger conducting housing, and a system of set screws and bolts allow the propellant module and an extractor electrode to be aligned relative to each other and fixed in the frame of the thruster.

To build our AFET-2, we followed largely the methodology of [3]. The thruster housing, propellant module housing, and distal electrode were all machined on a manual milling machine, and made respectively of aluminum, polyether ether

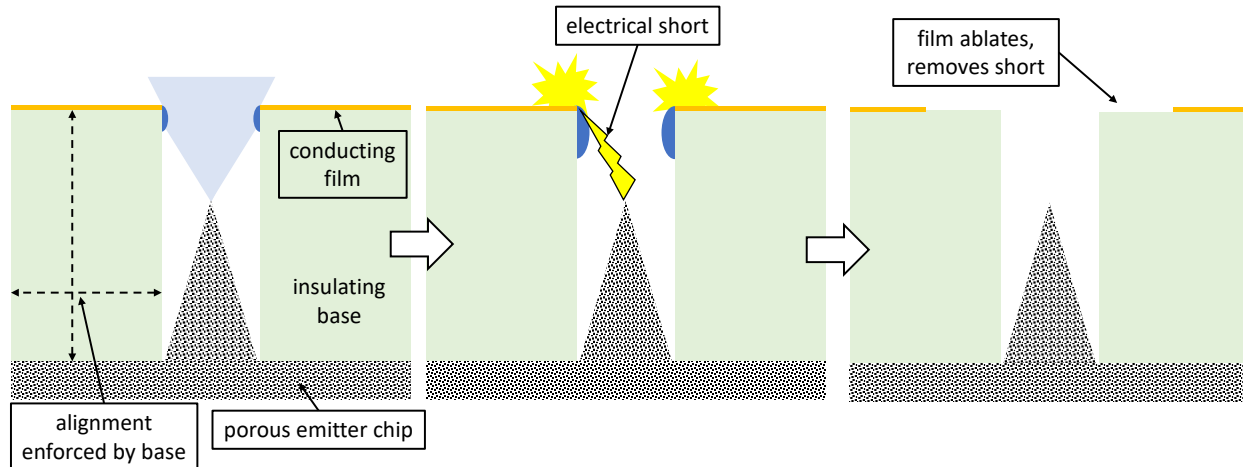


Fig. 1 Notional mechanisms of resilient extractor architecture.

ketone (PEEK) plastic, and 316L stainless steel. The emitter chip was machined from a P5 grade porous borosilicate glass frit, and the porous reservoir is a P4 frit (both ROBU Glasfilter-Geräte GmbH). The filter paper was Whatman Qualitative No. 1. The emitters were machined using a high-speed spindle (up to 30000 RPM) and were cut to be exactly pyramidal with a height of $\sim 320 \mu\text{m}$, though practically they are slightly shorter as a result of the rounding-off of the apices resulting from the machining.

We show in Fig. 2 pictures outlining the manufacturing process of the resilient extractor. First a piece of MACOR® ceramic (Corning Inc.) was fixtured to a block by cyanoacrylate glue and faced to desired thickness on the CNC using an end mill (a). After unbonding and cleaning the sample in an ultrasonic bath of acetone followed by a bath of isopropanol, a thin layer of silver was deposited on the substrate using a DC magnetron sputterer operating in an atmosphere of argon at a current of 30 mA for 6 minutes, resulting in a resistance of about 30Ω for probes measuring across a distance of 6 mm on the chip surface (b). The coated sample was then again fixtured to a sacrificial piece of MACOR, and a grid of $460 \mu\text{m}$ diameter apertures machined through the substrate using a miniature drill on the CNC mill (c). The chip profile was cut out of the MACOR substrate with the end mill (c), and the sample placed in a fresh acetone bath in the ultrasonic cleaner to unbond and clean. After doing so, a stainless steel frame to hold the extractor chip was machined on the CNC mill, and the chip was bonded into the frame with a conductive epoxy (MG Chemicals 8331) (d). The frame has the same profile as the baseline AFET-2 extractor electrode, except that a pocket (compare with the exploded view of Fig. 3) holds the chip and allows it to protrude from the face of the frame so that it can interface with the emitter chip.

Altogether, the machining process was unproblematic and fairly robust as a result of the substrate's ease of machining and stiffness. We display a micrograph of the completed extractor chip in Fig. 4. The only difficulties were thus: Firstly, that chipping around the aperture edges as a result of the functionally abrasive machining of the substrate necessitated narrowing the apertures compared to the normal AFET-2 extractor design, as otherwise the conductive film could be wholly interrupted in the webbing. And secondly, that due to operator error in setting the work coordinate system of the CNC mill, the sample was $70 \mu\text{m}$ thicker than intended ($390 \mu\text{m}$ instead of $320 \mu\text{m}$ to make the electrode flush with the emitter tips).

Notable in the construction of the chip is that it is flat to within about $6 \mu\text{m}$ and is quite rigid as a result of its thickness and the stiffness of the material. Indeed, the steel frame into which it is bonded is largely unnecessary to ensure that it remains globally flat, and instead it serves largely as a convenience to avoid having to manufacture a larger piece entirely from MACOR. Furthermore, this methodology is readily extensible to larger extractor chips.

C. Assembly and integration

Prior to testing, the propellant module was assembled, placed into the thruster housing, and loaded with 1-ethyl-3-methylimidazolium tetrafluoroborate (EMI-BF₄). The propellant was dried at high vacuum in a petri dish overnight and then deposited onto the the emitter chip and allowed to soak into the wettable thruster components again at high vacuum over a couple days. In between loading and testing, the loaded thruster was stored in a nitrogen-purged drybox, which

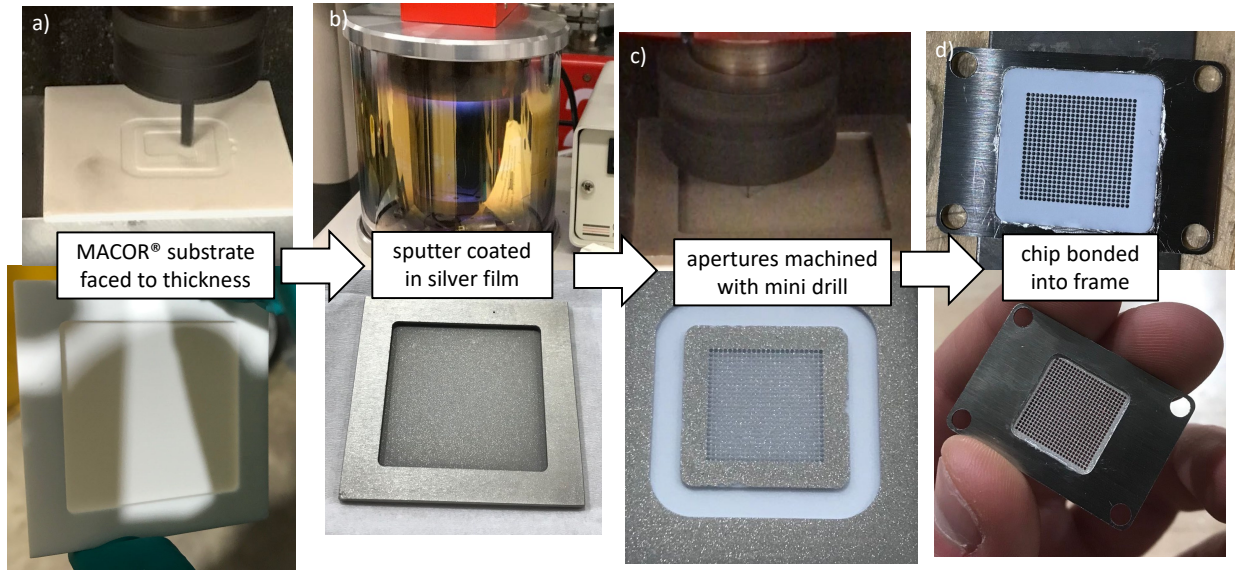


Fig. 2 Manufacturing process for resilient extractor: a) MACOR substrate machined to thickness on a CNC mill, b) sample coated in silver film using a DC magnetron sputterer, c) aperture grid machined with a miniature drill, and d) chip bonded into a support frame with conductive epoxy

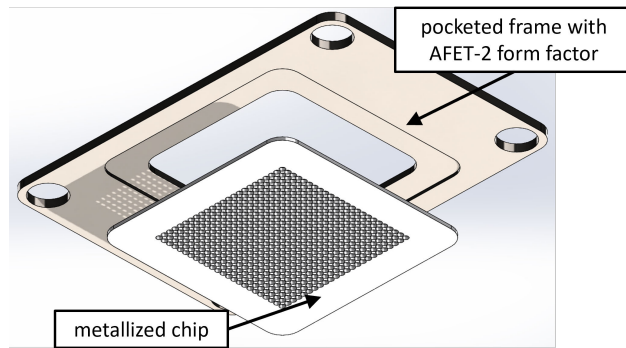


Fig. 3 Exploded view showing the pocketed frame into which the extractor chip seats; the metallized film contacts the frame through a conductive epoxy, while the far side is uncoated dielectric

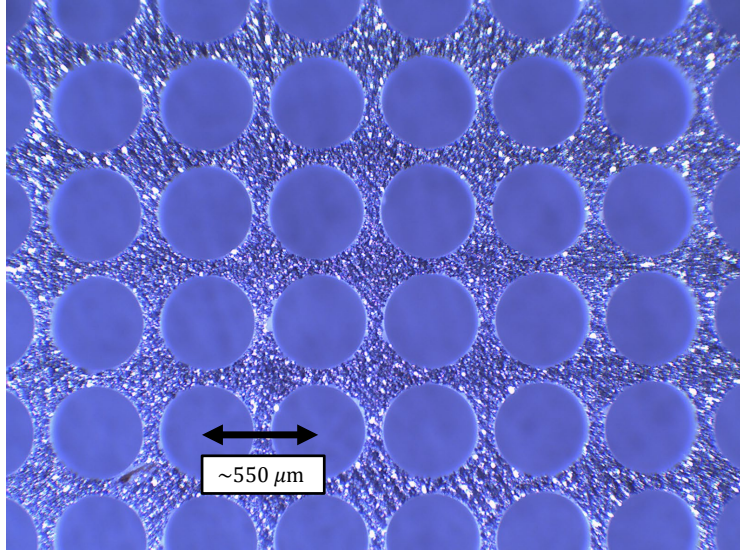


Fig. 4 Optical micrograph of the completed extractor chip

maintains a humidity of less than 1% as measured by a hygrometer. The propellant did not fully wet into the porous reservoir, and so to wick away the excess propellant, the propellant module was disassembled and the supersaturated emitter chip placed onto a KIMTECH® delicate task wipe in the drybox. In troubleshooting the wetting, the emitter chip sustained modest fractures, though these were localized solely in the base of the chip away from the actual array of emitters. Testing thus proceeded by mating the fractured pieces together while reassembling the propellant module.

With the propellant module loaded and assembled, we then installed the resilient extractor. Without adjusting the alignment set screws, the extractor chip sits above the level of the emitters to prevent accidentally breaking the emitter tips. To align the thruster laterally, we used a desktop optical microscope equipped with a CCD camera. In this configuration, the vertical stage of the microscope is adjusted to first focus on the top surface of the extractor and then on the tips of the emitters, with a micrograph taken at each. By fitting a circle to the apertures in the image capture software, we determined the offset between the emitter tips and aperture centers and adjusted the set screws to rotate and translate the extractor as necessary. A four-point stencil is used, one emitter in each corner, to verify alignment. An example alignment micrograph to identify the center of an aperture is shown in Fig. 5. After adjusting the set screws and securing the extractor into place, each point in the stencil was aligned to aperture center within 20 μm. After laterally aligning the thruster, the set screws underneath the thruster were adjusted in a star pattern to gradually raise the emitter chip to the bottom surface of the extractor, at which point a resistance is felt and the propellant module secured into place. We display a picture of the thruster after assembly and alignment in Fig. 6.

III. Experimental Setup

We operated the AFET-2 with the resilient extractor installed in the Plasmadynamics and Electric Propulsion Laboratory's (PEPL's) Electro Spray Thruster Array Chamber (ETAC). ETAC (Fig. 7) is a 0.81 by 1.22 m stainless steel vacuum chamber which achieves high vacuum by turbomolecular pump (Pfeiffer Vacuum TPH 1501 UPN). During all tests reported here, the pressure in the facility was 6-7 μTorr, as measured with an ionization gauge. An optical table is mounted on slides to provide a convenient platform for the assembly of experimental apparatus. The thruster is mounted on a stainless steel plate which is isolated from the table by a mica sheet and fiberglass composite interface. Voltage and current are sourced to the thruster by an Ultravolt HV Rack power supply configured for negative unipolar operation up to -4 kV and -370 μA. Power travels through an isolated HV pin that passes through the propellant module housing and contacts the distal electrode on its underside. A Keithley picoammeter (model 6485) is connected between the thruster mount and ground to determine the current collected by the extractor electrode and thruster body, to which it is electrically connected (i.e. as an assessment of propellant interception). A large Faraday probe consisting of a stainless steel plate connected in line with a power supply (Tenma 72-2715) and another model 6485 picoammeter is mounted on a set of translational motion stages such that the probe can be maneuvered to intercept the entirety of the ion beam. For

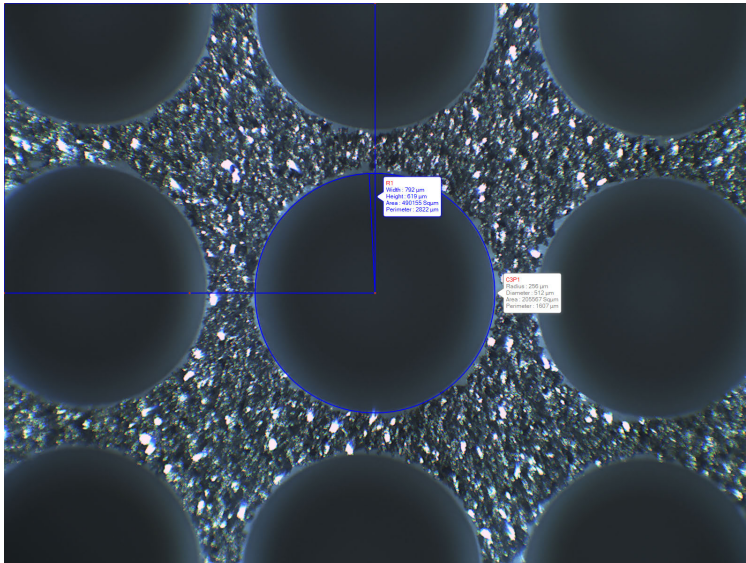


Fig. 5 Alignment micrograph to identify aperture center

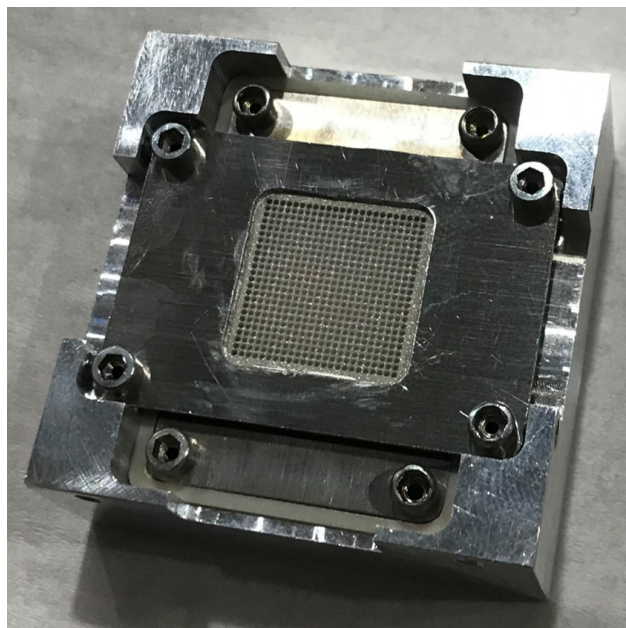


Fig. 6 The thruster fully assembled and aligned with the resilient extractor installed



Fig. 7 PEPL's ETAC vacuum facility

all experiments reported here, the plate was centered on the thruster and situated 2 cm downstream from the thruster face, subtending a half-angle of approximately 75 degrees. During testing, the in-line power supply was used to bias the probe to +40 V to recollect secondary species. Figure 8 is a picture of the experimental setup in the facility.

IV. Results

In this section, we present the results of thruster experiments operating with the resilient extractor prototype. We first provide I-V maps of the thruster and show a study of the conditioning of the thruster to steady operation. We then show images of the thruster after operation, including micrographs of the extractor chip.

A. Thruster conditioning and I-V map

We began testing the thruster by stepping the voltage from 0 to about -2700 V in 50 V increments, permitting 8-12 seconds of DC operation at a time, with the power supply output disabled and allowed to discharge in between. Measurable current was detected at the probe starting around -1000 V. We observed that, toward the beginning of thruster operation, and especially at higher voltages, the current emitted by the source decreased quickly over a few windows of operation, but began to level out at each voltage setpoint before stepping higher. After stepping up to -2700 V in this way, we then stepped the thruster down in voltage to -950 V, back to below where current was detected, again in 50 V increments. The maximum current emitted by the thruster over the course of this step-up was approximately $-190 \mu\text{A}$ at -2700 V. We show the emitted current for each of these points in Fig. 9.

After this preliminary exploration of the thruster operation space, we returned the thruster to -2450 V potential and conditioned the thruster, operating it again 8-12 seconds at a time, for 40 minutes, until the thruster reached a steady state of operation. We show in Fig. 10 the current collected by the probe and by the extractor sense line over the course of this conditioning. The current begins at $-36 \mu\text{A}$ and decays over the course of 7 minutes to $-21 \mu\text{A}$, where it remains, with some variance, thereafter. This conditioning may be the cause of the fluid in the thruster needing to achieve some equilibrium state (e.g. the presence of a fluid film external to the substrate that must be removed prior to operation). Aside from the initial operation where the extractor current is 1.3% of the emitted current, the extractor current is below the measurement resolution of the picoammeter for the chosen range ($<1 \text{ nA}$).

After conditioning the thruster to steady operation, we again took an I-V trace descending from -2700 V to -950 V in 50 V increments. We then turned off the thruster for an hour, at which point we restarted it at -2450 V. When restarting it after this rest period, there was again some conditioning required to bring the thruster back to steady operation there, but it took substantially less time than previously, only a few minutes. The probe current traces for both of these cases are shown alongside that taken before any conditioning in Fig. 9.

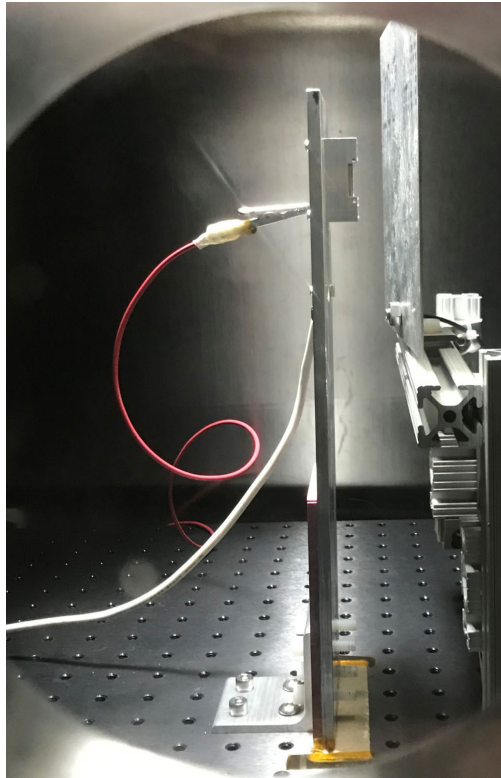


Fig. 8 Thruster, with resilient extractor installed, ready for testing; the red wire sources voltage and current to the emitters through an isolated pin, and the white wire senses the current into the body and extractor; the probe is pictured to the right

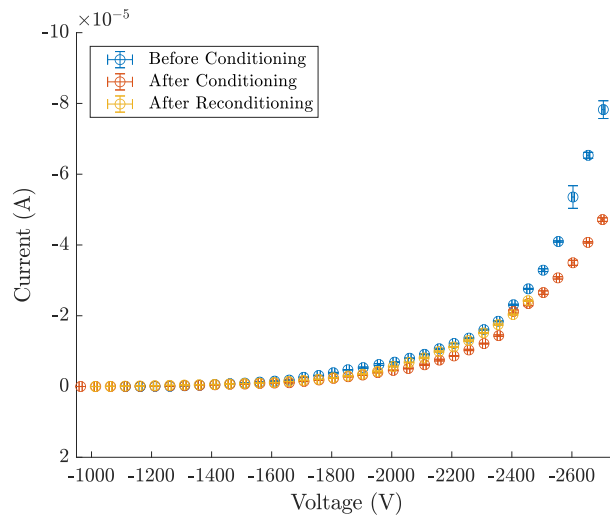


Fig. 9 Three I-V traces taken for the thruster: in blue, during an initial exploration of the thruster operation before conditioning the thruster; in orange, after conditioning the thruster to steady operation over 40 minutes at -2450 V; and in gold, after allowing the thruster to rest for an hour and reconditioning to steady state

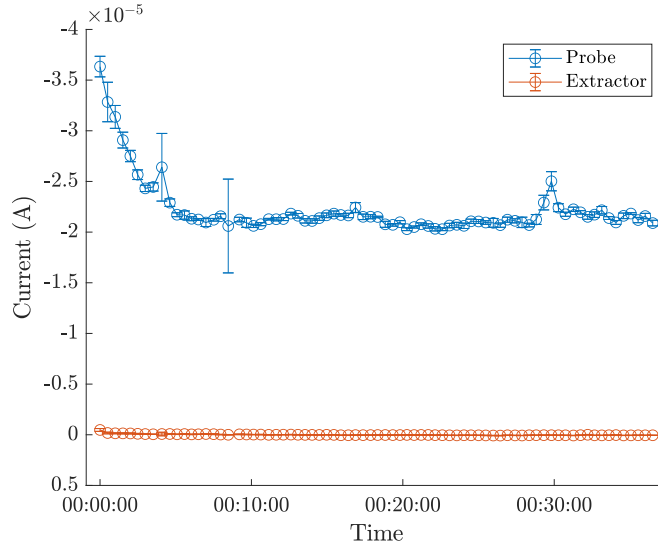


Fig. 10 Current emitted by the thruster as measured by a downstream probe (blue) operating at -2450 V over the course of a 40 minute thruster conditioning, along with the current sunk to the extractor and body (orange) over the same period; error bars represent a single standard deviation of the current signal over each 8-12 second test point

As is evident in the figure, the thruster sourced decidedly more current before having been conditioned down to steady state, though it converges with the other traces below about -1500 V. If conditioning is indeed consistent with removal of a film of excess propellant, it could be associated with transient operation in a regime of lower hydraulic impedance, resulting in higher current for the same voltage consistent with the analysis of [12, 16–18] and potentially even moving into a cone-jet mode. The latter two traces much more closely track each other, though there appears to be a step discontinuity between -2450 and -2300 V in the second case.

B. Extractor resiliency

After completion of the aforementioned tests, the thruster was removed from the vacuum chamber and inspected under an optical microscope. The thruster face was noticeably discolored, adopting a brownish hue (see Fig. 11). Microscope images of the extractor revealed there were noticeable deposits of propellant around 8% of the apertures. We show in Fig. 12 an indicative micrograph of one such aperture. The deposit is a dark brown color, indicating possible carbonization from heat, and is concentrated at the edge of the aperture. Noticeably, the silver film has been removed in a perimeter surrounding the deposit, found to be universally true across the extractor chip. This indicates, then, that there is not a conduction path through the carbonized propellant, that is, that the removal of the film has resulted in elimination of a potential short.

V. Discussion

In this section, we discuss the preceding results within the three fundamental aims of the resilient extractor architecture. The first is an examination of whether the extractor succeeds in ease of manufacture and in aiding alignment. Secondly, we examine whether the extractor exhibited the targeted resilient behavior. Finally, we discuss how similarly the electrode functions to a more baseline extractor configuration.

A. Ease of manufacture and alignment

The first key aim of this architecture was to aid in the assembly and alignment of the thruster, and in this respect the prototype was largely successful. By manufacturing the chip to a fixed thickness, it became trivial to ensure proper vertical alignment in assembling the thruster; after mating the extractor to the emitter chip, the height offset was measured to be within 10 μm of the thickness of the extractor. Correspondingly, the tolerance in alignment is directly

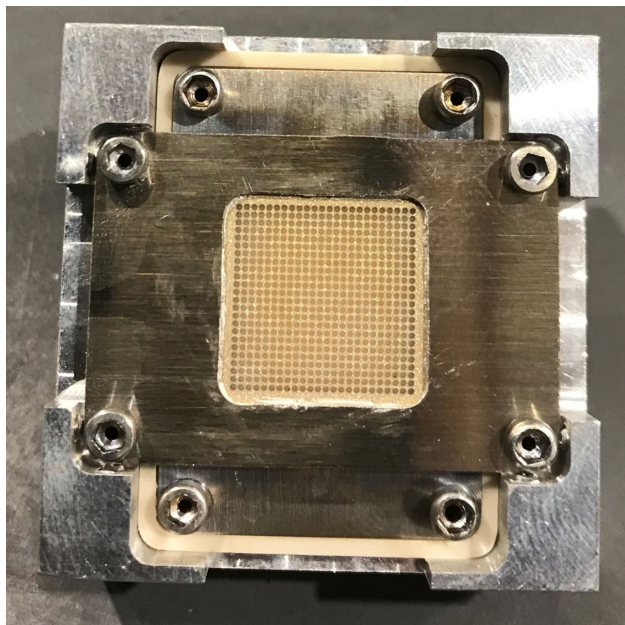


Fig. 11 Thruster face after operation, with noticeable discoloration

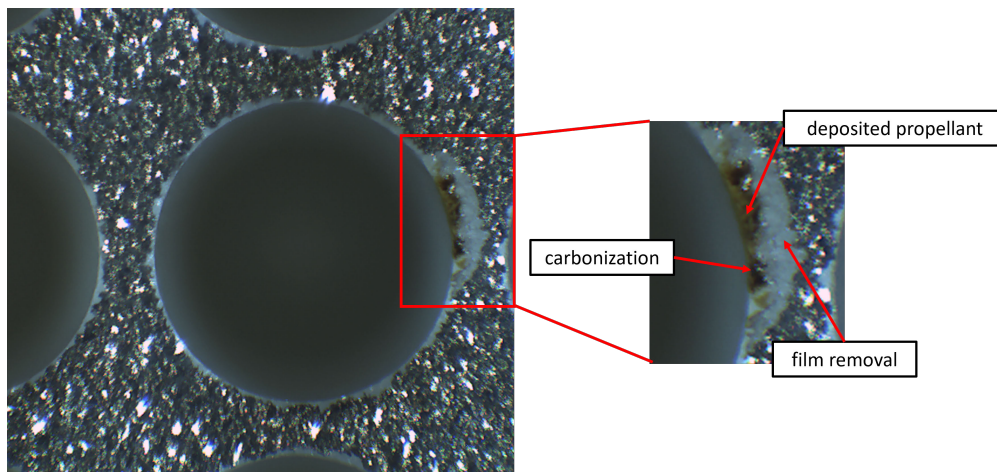


Fig. 12 Propellant deposit on extractor face, with evident carbonization and removal of the silver film

predicated on the tolerance in the extractor thickness and on the flatness of the emitter chip basal plane, eliminating potential accumulated errors from other structural elements. For systems like the AFET-2 where vertical alignment is performed by adjusting the relative position of the components, this also represents a simplification of this process, though it does eliminate the ability to parametrically investigate the effect of this offset on performance, unless the extractor is allowed to sit off the thruster face akin to a more standard configuration. Additionally, while here we ensured horizontal alignment by manual adjustment, this is also possibly done through the architecture. The simplest method of doing so would be to design apertures of a radius near that of the base radius of the emitters, such that the extractor slides down and on top of them. However, this is a structural risk to the emitters and heavily constrains the design space, so instead we can envision an approach in which we machine a circular base on which each emitter sits that is instead used as an alignment feature.

These advantages are key within the context of scaling these devices to higher power. By structurally grounding the extractor to the emitter chip, flexure in the extractor is essentially eliminated. This is the result both of the additional support offered by the chip and the greater permissible thickness in the extractor, to the order of the emitter height for the same relative positioning of the electrode. Indeed, we had great difficulty in attempting to machine an extractor consistent with the methodology of [3], as during machining stresses were often sufficient to induce warping in the metal. The only sources of inhomogeneity in alignment are thus the tolerances of the manufacturing processes. Here, we manufactured the resilient extractor prototype using only a CNC mill and the DC magnetron sputter, both readily available in a research or industrial settings. With judicious maintenance and setup, such conventional machining can achieve positional accuracy of order $0.1 \mu\text{m}$ per mm, meaning a $10 \mu\text{m}$ positional tolerance would correspond to a system 100 mm in scale. Indeed, this scale is the practical limit of the process used in this study, being the maximum sample size accommodated by the sputterer. For the $O(1W)$ operation of the AFET-2 [3] or similar systems [5, 6], this scale would correspond to a device of around 30 W power.

B. Extractor resiliency

We last discuss the resiliency of the extractor. As evidenced by Fig. 12, over the course of operation of the thruster, propellant was deposited onto the electrode. These deposits were heavily concentrated at the lip of the apertures, from which we conclude that their origin is largely from within the aperture itself, and not as resulting from some secondary species reabsorbed from the facility. Furthermore, the carbonized nature of these deposits suggests that they carried current at some time, whether through a direct propellant bridge to the emitter or as a result of some backspray type phenomenon [1, 13, 19]. However, we note that, through course of these experiments, there was never a gross short between the electrodes (i.e., one that caused the power supply to enter a current-controlled mode). There were on occasion, particularly during the initial voltage ramp of the thruster and its subsequent conditioning, small-magnitude current transients visible on the extractor, of order no more than 10% of the beam current. These may be short-lived shorts, indicating that such obstructions are removed on a time scale smaller than that of our data collection, which averaged over about 100 ms of current collection with the picoammeters. In concert, these observations suggest that the extractor succeeded in ablating local to the propellant deposits when a short occurred, and that this short was cleared quickly, without significant perturbation of the thruster.

With that said, we note that these deposits may not result directly from emission, but rather from migration of propellant up along the walls, since the extractor directly contacts the emitter chip. However, given the flatness of the extractor and of the basal plane of the emitter chip we would expect such a phenomenon to occur at all apertures across the emitter array at a similar time, and for it to be perhaps uniformly distributed about the aperture, which we found not to be the case. Additionally, we have observed similar deposits to those seen here in operating the thruster with a more conventional AFET-2 extractor, which lacks this potential fluidic path. Combined with the lack of intense electrical traction because the electric field in the vicinity of the wall and the emitter basal plane is substantially weakened due to its lack of field amplification effect and the nearby presence of the dielectric substrate, we do not believe this to have been a contributing mechanism to the propellant deposits. If it were, one could imagine laminating also a thin layer of non-wetting material such as polytetrafluoroethylene (PTFE) underneath to further discourage such a process.

C. Incongruence of device operation

These experiments indicate successful operation of the AFET-2 system with the resilient extractor prototype inasmuch as the thruster was able to source current into a beam and that very little (<1%) of this beam was intercepted by the extractor. There is qualitative agreement with prior results reported for the AFET-2 [3] for the I-V map in its characteristically inflected current response. However, quantitatively our thruster sourced nearly an order of magnitude

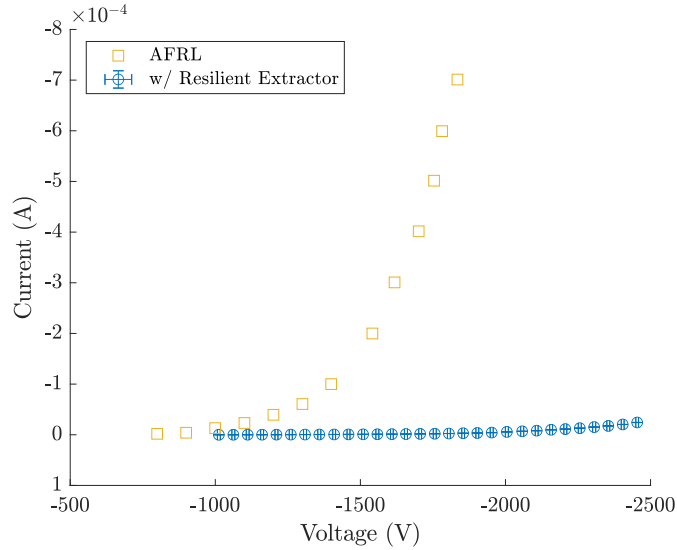


Fig. 13 Data of the final I-V Map taken in this work (blue circles) compared with the I-V map reported in [3] (yellow squares)

less than that of [3], as highlighted in Fig. 13 (about $-50 \mu\text{A}$ at -2450 V compared to about $-700 \mu\text{A}$ at -1850 V). We believe this discrepancy to be the result of different levels of field amplification in each device. That is, insofar as the current sourced by the device is controlled by the Taylor cone dynamics, and these themselves are controlled by the local electric pressure [9, 16–18, 20], for two systems for which the mapping between applied voltage and electric field at the emitter tips disagrees but are otherwise identical, to first order their I-V curves should be linear scaling in the voltage. To this end, we show in Fig. 14 another chart where the data observed in this work are scaled down by a factor 2.2 in voltage. As is evident in the figure, at least over this limited range of data, this simple linear scaling appears to account for the performance discrepancy, suggesting that the electric field in the resilient extractor configuration is substantially weaker.

There are several potential causes of this weaker field. The additional $70 \mu\text{m}$ of electrode gap from human error in manufacturing should in principle weaken the field; however, simulations of the two different geometries for the baseline AFET-2 extractor architecture using the electrostatic model of [12] suggest this should be a small effect, causing only an 8% discrepancy. This is because this offset is small on the scale of the aperture radius, and so doesn't represent a large change in the total separation between the electrodes. Another possible explanation is the presence of the dielectric base. Kimber *et al* reported electrostatic simulations for which the presence of a dielectric base in a similar architecture resulted in a weakening of the electric field [21]. These results, however, were for a configuration where the emitter was deeply embedded within the dielectric substrate, whereas the configuration of the AFET-2 and similar systems, including those with dielectric-coated extractors [5, 6], typically place emitter tips flush with the extraction electrode, such that we would anticipate this to be a smaller effect. As a final explanation, and what we believe to be the most likely, the disparity in IV curve may be attributed to differences in the sharpness of the emitter tips for our system versus the previously reported AFET-2 design. The microscope used in this study was not capable of measuring the tip radii as a result of its short working distance, but previous results have highlighted the sensitivity of the local electric field to the curvature of the tip [12]. Indeed, at this scale, a factor two discrepancy in the tip curvature is sufficient to produce the approximately factor two discrepancy in the electric field observed here, indicating we may possess a population of emitters of radius $20+ \mu\text{m}$, in contrast to the $10\text{-}20 \mu\text{m}$ reported in [3]. This may be a result of the smaller spindle speed achievable in this work (30000 RPM instead of 50000) or be a consequence of greater runout in the spindle.

VI. Conclusion

The goal of this work was to experimentally validate a concept for a resilient extractor consisting of a metallized dielectric interfaced directly with the emitter chip. The prototype considered here succeeded in simplifying and reducing potential error in thruster alignment and ablating to remove shorts, consistent with its conception of operation:

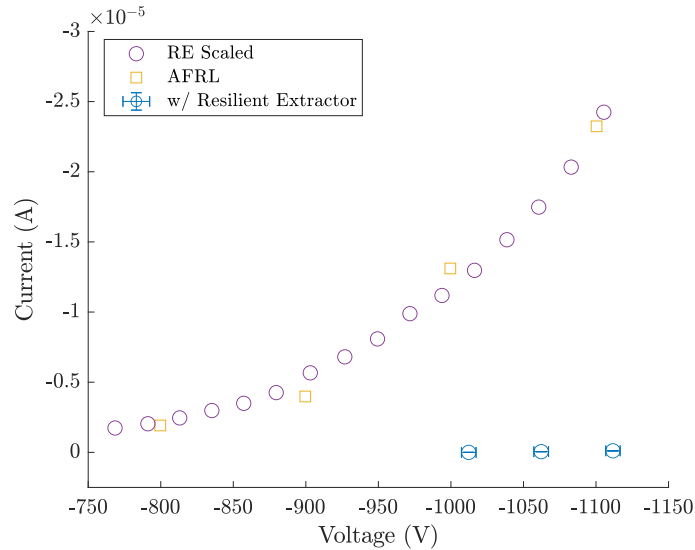


Fig. 14 Subsection of Fig. 13, also with data for the resilient extractor scaled by a factor 2.2 in voltage (purple circles)

Approximately 8% of apertures had evidence of propellant deposition, but the resilient extractor succeeded in ablating surrounding this deposition and thruster operation continued; through the rigid construction of the dielectric base, we found it comparatively easy to align the extractor vertically within 10 μm of its thickness; and finally, though the current sourced by the thruster is less than 10% of that previously reported for an AFET-2, this discrepancy is likely explained by decreased field amplification resulting from duller emission tips. Altogether, the properties of this architecture provide several potential benefits for electrospray systems, especially when considering the problem of aggregating significantly more emitters to reach higher powers, including potential alignment inhomogeneities and the interrelated but more pernicious problem of thruster-disabling electrode shorts.

Acknowledgements

The authors would like to acknowledge support for this work in the form of an Educational Partnership Agreement with the Air Force Research Laboratory, Edwards and also a NASA Space Technology Graduate Research Opportunity (80NSSC21K1247). We also wish to thank the department instrument maker Mr. Terry Larrow for fabricating the thruster and propellant module housings and Ruowen Tu for his aid in operating the DC magnetron sputterer.

References

- [1] Ziemer, J., Marrese-Reading, C., Dunn, C., Romero-Wolf, A., Cutler, C., Javidnia, S., Le, T., Li, I., Franklin, G., Barela, P., Hsu, O., Maghami, P., O'Donnell, J., Slutsky, J., Thorpe, J. I., Demmons, N., and Hruby, V., "Colloid Microthruster Flight Performance Results from Space Technology 7 Disturbance Reduction System," *International Electric Propulsion Conference*, 2017, p. 578.
- [2] Lozano, P. C., Wardle, B. L., Moloney, P., and Rawal, S., "Nanoengineered thrusters for the next giant leap in space exploration," *MRS Bulletin*, Vol. 40, No. 10, 2015, p. 842–849.
- [3] Natisin, M. R., Zamora, H. L., McGehee, W. A., Arnold, N. I., Holley, Z. A., Holmes, M. R., and Eckhardt, D., "Fabrication and characterization of a full conventionally machined high-performance porous-media electrospray thruster," *Journal of Micromechanics and Microengineering*, Vol. 30, 2020, p. 115021.
- [4] Legge, R. S., and Lozano, P. C., "Electrospray Propulsion Based on Emitters Microfabricated in Porous Metals," *Journal of Propulsion and Power*, Vol. 27, No. 2, 2011, pp. 485–495.
- [5] Krejci, D., Mier-Hicks, F., Fucetola, C., Lozano, P., Schouten, A. H., and Martel, F., "Design and Characterization of a Scalable Ion Electrospray Propulsion System," *International Electric Propulsion Conference*, 2015, p. 149.

- [6] Petro, E., Bruno, A., Lozano, P., Perna, L. E., and Freeman, D., "Characterization of the TILE Electro spray Emitters," *AIAA Propulsion and Energy 2020 Forum*, 2020, p. 3612.
- [7] Courtney, D. G., Alvarez, N., and Demmons, N., "Electro spray Thrusters for Small Spacecraft Control: Pulsed and Steady State Operation," *2018 Joint Propulsion Conference*, 2018, p. 4634.
- [8] Perez-Martinez, C., and Lozano, P., "Ion field-evaporation from ionic liquids infusing carbon xerogel microtips," *Applied Physics Letters*, Vol. 107, No. 4, 2015, p. 043501.
- [9] St.Peter, B., Dressler, R. A., Chiu, Y.-H., and Fedkiw, T., "Electro spray Propulsion Engineering Toolkit (ESPET)," *Aerospace*, Vol. 7, No. 91, 2020.
- [10] Fedkiw, T. P., Wood, Z. D., and Demmons, N., "Improved Computed Tomography Current Mapping of Electro spray Thrusters," *AIAA Propulsion and Energy 2021 Forum*, 2021, p. 3389.
- [11] Demmons, N., Margousian, A., Knott, J., Alvarez, N., D'Amato, D., and Ziemer, J., "Life-Limiting Factors of the CMTS for Precision Pointing Observatory Missions," *AIAA Propulsion and Energy 2021 Forum*, 2021, p. 3403.
- [12] Whittaker, C. B., Gorodetsky, A. A., and Jorns, B. A., "Model Inference on an Electro spray Thruster Array," *AIAA 2022 SciTech Forum*, 2022, p. 0041.
- [13] Thuppul, A., Wright, P. L., and Wirz, R. E., "Lifetime Considerations and Estimation for Electro spray Thrusters," *2018 Joint Propulsion Conference*, 2018, p. 4652.
- [14] Jorns, B. A., Gorodetsky, A., Lasky, I., Kimber, A., and Dahl, P., "Uncertainty Quantification of Electro spray Thruster Array Lifetime," *International Electric Propulsion Conference*, 2019, p. 317.
- [15] Gorodetsky, A., Whittaker, C. B., Szulman, A., and Jorns, B., "Robust Design of Electro spray Emitters," *AIAA Propulsion and Energy 2021 Forum*, 2021, p. 3422.
- [16] Coffman, C., Martinez-Sanchez, M., Higuera, F., and Lozano, P. C., "Structure of the menisci of leaky dielectric liquids during electrically-assisted evaporation of ions," *Applied Physics Letters*, Vol. 109, No. 23, 2016, p. 231602.
- [17] Coffman, C. S., Martínez-Sánchez, M., and Lozano, P. C., "Electrohydrodynamics of an ionic liquid meniscus during evaporation of ions in a regime of high electric field," *Physical Review E*, Vol. 99, 2019, p. 063108.
- [18] Gallud, X., and Lozano, P. C., "The emission properties, structure and stability of ionic liquid menisci undergoing electrically assisted ion evaporation," *Journal of Fluid Mechanics*, Vol. 933, 2022, p. A43.
- [19] Wright, P. L., Thuppul, A., and Wirz, R. E., "Lift-Limiting Emission Modes for Electro spray Thrusters," *2018 Joint Propulsion Conference*, 2018, p. 4726.
- [20] Wright, P. L., and Wirz, R. E., "Multiplexed electro spray emission on a porous wedge," *Physics of Fluids*, Vol. 33, 2021, p. 012003.
- [21] Kimber, A., Jorns, B., and Sodano, H., "Dielectric Materials with Deposited Electrode Layers for Electro spray Arrays," *2018 Joint Propulsion Conference*, 2018, p. 4653.